nature nanotechnology

FOCUS | REVIEW ARTICLE

PUBLISHED ONLINE: 6 JANUARY 2015 | DOI: 10.1038/NNANO.2014.311

Plasmon-induced hot carrier science and technology

Mark L. Brongersma[1,2]*, Naomi J. Halas[3]* and Peter Nordlander[3]*

The discovery of the photoelectric effect by Heinrich Hertz in 1887 set the foundation for over 125 years of hot carrier science and technology. In the early 1900s it played a critical role in the development of quantum mechanics, but even today the unique properties of these energetic, hot carriers offer new and exciting opportunities for fundamental research and applications. Measurement of the kinetic energy and momentum of photoejected hot electrons can provide valuable information on the electronic structure of materials. The heat generated by hot carriers can be harvested to drive a wide range of physical and chemical processes. Their kinetic energy can be used to harvest solar energy or create sensitive photodetectors and spectrometers. Photoejected charges can also be used to electrically dope two-dimensional materials. Plasmon excitations in metallic nanostructures can be engineered to enhance and provide valuable control over the emission of hot carriers. This Review discusses recent advances in the understanding and application of plasmon-induced hot carrier generation and highlights some of the exciting new directions for the field.

The photoelectric effect was discovered by Heinrich Hertz in 1887 while studying the effects of ultraviolet light on electrical discharge from metallic electrodes[1]. The key explanation of the phenomenon was provided in 1905 by Albert Einstein[2]. He suggested[3] that a beam of light consists of a set of discrete wavepackets (photons), each with a quantized energy E linked to their frequency ν by Planck's constant h ($E = h\nu$). This bold proposal explained why, below a certain threshold frequency, light cannot eject an electron from a metal surface, regardless of the intensity. The process requires a minimum photon energy equal to the metal's work function. These historical events provided the initial sparks for the quantum revolution and spurred a tremendously diverse set of fundamental research efforts aimed at elucidating the complex physical, electrical, thermal, mechanical and chemical processes that can be stimulated with energetic, photoexcited 'hot' electrons. Figure 1 illustrates the wealth of possible hot electron effects.

The photoemission process (Fig. 1a), in which the energy of an incident photon is used to eject an electron, is arguably the most well-studied phenomenon involving hot electrons. The energy and angular dependence of the photoemitted electrons provide important information about the electronic structure and the surface properties of solids[4]. Typically only a small fraction of photoexcited hot electrons make it out of a material, because the ejection process competes with very fast carrier relaxation processes. The section on 'Photoemission and ultrafast optical studies' briefly reviews our current understanding of hot electron excitation, relaxation, transport and photoejection mechanisms.

The excitation of an electron in a solid results in two types of carrier: an electron and a hole. These carriers are considered 'hot' if their energies are larger than those of thermal excitations at ambient temperatures. The branching ratios of hot/cold electron/hole formation depend on the electronic structure and photon energy[5]. Both types of hot carrier stimulate useful physical or chemical processes, but their ability to do so is limited by rapid relaxation processes by which the carrier's energy is converted into heat. On the flip side, carrier relaxation provides an opportunity to heat nanostructures effectively (Fig. 1b). The ability to stimulate and control local heating has many practical applications, which are discussed in the section on 'Local heating with hot carriers'.

Hot carriers can have positive or negative energy depending on their position with respect to the vacuum level. The negative-energy hot electrons are bound to the nanostructure but can have energies that are much larger than those arising from thermal excitations. As such, they are of particular importance in chemical and charge transfer applications. Such electrons can transfer into unoccupied levels of acceptor molecules in nearby structures and induce, for example, photochemical transformations (Fig. 1c) or photo-desorption (Fig. 1d). This insight has recently enabled the design and development of new photochemical processes that offer high levels of spatial and temporal control over chemical reactions. These are discussed in the section on the 'Applications of hot carriers in chemistry'.

Finally, there is an opportunity to harvest the hot carriers for a number of device applications (Fig. 1e,f), as discussed in the section on 'Hot carrier devices' where we focus on photodetection rather than photovoltaics, as the latter topic has recently been reviewed[6].

At the birth of each photogenerated hot carrier is a photon absorption event. Plasmonics provides ways to manipulate light absorption with nanometre-scale precision and at sub-femtosecond timescales enabling new levels of control of hot carrier processes. We provide an outlook for the outstanding opportunities in this regard at the end of the Review.

Photoemission and ultrafast optical studies

The illumination of a metallic structure sets off a cascade of complex processes that can have multiple outcomes, including the ejection or fast internal relaxation of hot carriers, the production of strong optical near fields and/or the (re-)emission of a photon. Our understanding of these processes has benefited from the field of surface femtochemistry, which became an intense research area in the 1990s. The first step in the excitation of a hot carrier is the absorption of a photon (Fig. 2a). The probability for photon absorption is proportional to the square of the local electric field inside the metal. Planar metal surfaces reflect most of the incident light, and light absorption is not very efficient. Early photoemission studies on metallic films revealed the importance of plasmon resonances to enhance light absorption in the near-surface region of the metal and thereby to enhance the photoemission[7,8]. In metallic nanostructures,

[1]Geballe Laboratory for Advanced Materials, Stanford University, Stanford, California 94305, USA. [2]Stanford Institute for Materials and Energy Sciences, SLAC National Accelerator Laboratory, 2575 Sand Hill Road, Menlo Park, California 94025, USA. [3]Laboratory for Nanophotonics, Department of Electrical and Computer Engineering, Department of Physics and Astronomy, and Department of Materials Science and Nanoengineering, Rice University, Houston, Texas 77005, USA. *e-mail: Brongersma@stanford.edu; halas@rice.edu; nordland@rice.edu

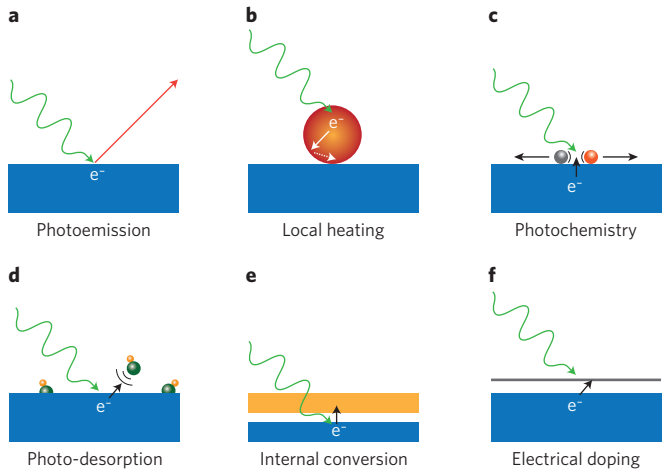

Figure 1 | Effects that can be stimulated by the photoexcitation of hot electrons in a metal (blue). a, Photoemission of electrons from a metal surface into vacuum can occur when the electron energy exceeds the metal's work function. **b**, Photoexcited hot electrons can remain trapped inside a metallic nanostructure and cause local heating of a metal particle (red) and its surroundings. **c**, Hot electrons can interact with molecules on a surface and induce photochemistry. **d**, The energy of hot electrons can be used to photo-desorb small molecules from the surface. **e**, Photoejected electrons from a metal can be captured by a counter-electrode (orange) to generate useful current. **f**, Photoejected electrons can be captured by an ultrathin semiconductor layer or two-dimensional materials (grey) and electrically dope them.

light absorption can be further enhanced by exciting localized surface plasmon resonances. This produces an antenna effect resulting in light collection from an area that is larger than its physical size[9,10]. The associated light concentration has been verified by and used in surface-enhanced processes, including surface-enhanced Raman spectroscopy[11], in photochemistry on surfaces[12], and to photoexcite nearby quantum emitters[13].

Plasmon resonances in nanostructures can be damped radiatively by re-emission of a photon or non-radiatively through the creation of hot electron–hole pairs via Landau damping (Fig. 2b)[14]. The branching ratio between these two decay mechanisms is determined by the radiance of the plasmon mode, which can be suppressed for structures supporting subradiant (dark) plasmon modes[15]. Landau damping is a pure quantum mechanical process in which a plasmon quantum is transferred into a single electron–hole pair excitation on a timescale τ_L ranging from 1 to 100 fs. The plasmon-induced electric field, which represents a time-dependent perturbation on the conduction electrons of the metal, can induce transitions of electrons from occupied to unoccupied states. As the transition matrix elements for electron–hole pair formation are small, however, the most probable immediate result of plasmon decay is the formation of a single electron–hole pair. A possible carrier distribution is illustrated in Fig. 2b. The distribution of the carriers depends on the plasmon energy, the particle size, the symmetry of the plasmon mode, and the electronic structure and density of states of the material[5]. Landau damping is the physical mechanism that contributes to the imaginary part of the dielectric permittivities of a metal in the visible. A knowledge of the imaginary part of the permittivity thus provides a means for optimizing hot carrier generation. For instance, by tuning a subradiant plasmon mode to energies where the imaginary part of the permittivity is large, it is possible to maximize the hot carrier production. This tuning can be performed either by exploiting the unique geometrical tunability of localized surface plasmon resonances (LSPRs) of metallic nanoparticles, or by fabricating composite structures consisting of both noble metals and metals with strong intraband transitions (such as transition metals). For plasmon energies above the interband transition threshold, the dominant portion of the hot carriers will be hot holes formed at the upper edge of the noble metal *d* band with the electrons located just above the Fermi level.

Since the work functions of standard plasmonic metals are larger than their LSPR energies $\hbar\omega_{LSPR}$, hot electrons will have negative energies ranging from the Fermi level E_F up to $E_F + \hbar\omega_{LSPR}$ and cannot escape into vacuum. The hot electrons generated from plasmon decay will quickly redistribute their energy among many lower-energy electrons via electron–electron scattering processes such as Auger transitions[16]. Although the dynamics of hot carrier relaxation processes have been extensively studied for extended surfaces, very little is known about this process in nanoscale systems. For extended metal surfaces, time-resolved studies[17,18] suggest relaxation times τ_{el} around 100 fs to 1 ps for formation of a Fermi–Dirac-like distribution characterized by a large effective electron temperature T_{el} (Fig. 2c). With the reduced velocity of these lower-energy electrons, interactions with the phonons increase. The subsequent equilibration with the lattice, which is characterized by a lattice temperature T_L, occurs over a longer timescale τ_{ph} of several picoseconds. The dynamics of this process can be well described using the so-called two-temperature model where T_{el} and T_L now become time-dependent and eventually equal[19]. In a final step, heat is transferred to the surroundings of the metallic structure. This can take from 100 ps to 10 ns depending on the material, the particle size and the thermal conduction properties of the environment (Fig. 2d).

For higher photon energies, a small fraction of hot electrons can also be emitted without energy loss. Advanced surface analytical techniques, such as angle-resolved photoemission spectroscopy can measure both the kinetic energy and momentum of the ejected electrons[20], in turn providing information on the energy and momentum of the electrons inside a material. For example, it is possible to measure directly the band dispersion (Fermi surface), and study complex many-body interactions in solids (Fig. 2e). By following the trajectories of photoemitted electrons created by intense laser pulses, researchers have also been able to analyse the evanescent fields around plasmonic nanoparticles. Because electrons are preferentially emitted from regions of high field intensity (hot spots) and subsequently accelerated within the evanescent fields of the plasmonic nanoparticles, they are steered in a direction determined by particle geometry (Fig. 2f)[21].

Applications of hot carriers in chemistry

Initial interest in hot-carrier-induced chemical reactions of adsorbates on photoexcited metal surfaces was stimulated by three distinct areas of research. Femtochemistry studies using well-defined single-crystal metal surfaces under ultrahigh-vacuum conditions led to reports of chemical reaction pathways specific to femtosecond laser excitation, with reaction products that were clearly distinct from thermal, phonon-mediated processes[19,22–24]. The desire to transfer this insight to real-world catalysts drove the adoption of metal nanoparticles rather than surfaces with specific index faces[16]. Independently, the discovery of photochemical water splitting on TiO_2 electrodes using ultraviolet light[25] led to intense interest in species that could be added to semiconducting metal oxides to enhance light absorption in the visible region of the spectrum. The large absorption cross-sections of plasmon-resonant noble metal nanoparticles were particularly attractive for modifying the optical properties of metal oxides. Studies of charge transfer between metallic nanoparticles and surrounding metal oxides subsequently emerged[26]. The discovery of surface-enhanced Raman spectroscopy[11] led to additional speculation as to whether direct plasmonic excitation could provide a pathway for enhanced photochemistry of adsorbate molecules at nanoparticle surfaces[27,28].

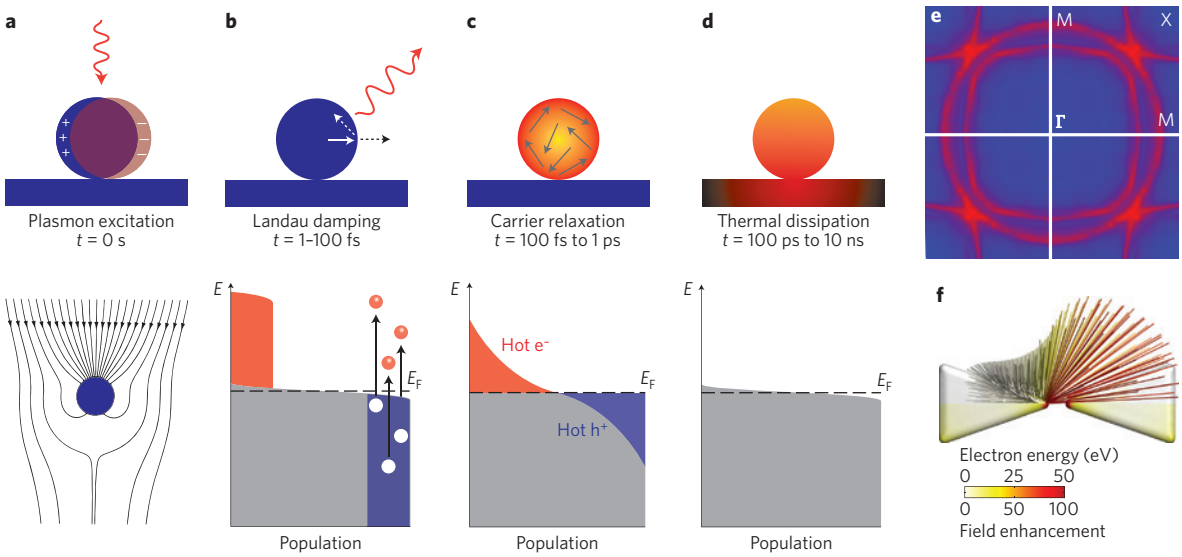

Figure 2 | Photoexcitation and relaxation of metallic nanoparticles. a–d, Photoexcitation and subsequent relaxation processes following the illumination of a metal nanoparticle with a laser pulse, and characteristic timescales. **a**, First, the excitation of a localized surface plasmon redirects the flow of light (Poynting vector) towards and into the nanoparticle. **b–d**, Schematic representations of the population of the electronic states (grey) following plasmon excitation: hot electrons are represented by the red areas above the Fermi energy E_F and hot hole distributions are represented by the blue area below E_F. **b**, In the first 1–100 fs following Landau damping, the athermal distribution of electron–hole pairs decays either through re-emission of photons or through carrier multiplication caused by electron–electron interactions. During this very short time interval τ_{nth}, the hot carrier distribution is highly non-thermal. **c**, The hot carriers will redistribute their energy by electron–electron scattering processes on a timescale τ_{el} ranging from 100 fs to 1 ps. **d**, Finally, heat is transferred to the surroundings of the metallic structure on a longer timescale τ_{ph} ranging from 100 ps to 10 ns, via thermal conduction. **e**, Fermi surface of a Sr_2RuO_4 single crystal surface in reciprocal space (showing the major symmetry points M, X and Γ) measured by analysing the energy and momenta of photoemitted electrons. **f**, Simulation of field enhancement in a plasmonic bow-tie structure, and the resulting electron trajectories. The length of the bow-tie antenna is 160 nm. Figures adapted with permission from: **a**, ref. 9, © 1983 American Association of Physics Teachers; **e**, ref. 20, © 2000 American Physical Society; **f**, ref. 21, © 2013 American Chemical Society.

In their transient higher-energy states, hot electrons can excite electronic or vibrational transitions in molecules adsorbed on metal surfaces and thus catalyse chemical reactions. The basic mechanism is illustrated in Fig. 1c,d. On extended metal surfaces, the timescale τ_{nth} is too short for the initial non-thermal hot electron distribution to have a significant effect on the adsorbate. Hot-electron-induced chemistry for such extended structures therefore most probably occurs after the high-effective-temperature Fermi–Dirac electron distribution has formed (Fig. 2c). Because the Fermi–Dirac distribution involves a continuous energy distribution of excited electrons (and holes) around the Fermi level, $E_F \pm k_B T_{el}(t)$, only adsorbate resonances in the vicinity of the Fermi level can be populated. Thus state-selective population of specific adsorbate resonances cannot be accomplished on extended metal surfaces[29]. This conclusion is supported by many experimental studies showing that there is typically no significant wavelength dependence for surface femtochemistry reactions on metal surfaces. In contrast, on metallic nanoparticles the lifetimes of the initially generated non-thermal hot electrons can be substantially longer because of increased confinement, more granular density of states and reduced electron–electron interactions[5,16]; also, the equilibration time with the lattice is longer because of reduced electron–phonon coupling. For example, in a study of small Ag particles on graphite, τ_{nth} was found to be approximately 2 ps (ref. 30). Thus for finite nanoparticles we expect a much larger number of high-energy hot carriers than on extended surfaces, and this may allow state-selective population of adsorbate resonances. This process provides a mechanism for the creation of negative-ion states of adsorbed or nearby molecules that can then undergo subsequent chemical transformations, as recently observed during plasmon-induced dissociation of H_2 on Au nanoparticles[31,32]. This scenario can be generalized: by populating specific antibonding adsorbate resonances, it may be possible to selectively induce desorption, dissociation or translational motion of adsorbates on a metal nanoparticle surface.

Equally important is the generation of hot holes following surface plasmon excitation of metallic nanoparticles, as these carriers become available for electron transfer from the highest occupied molecular orbital level of an adsorbate to the metallic nanoparticle. For example, hot holes can induce oxidation of citrate molecules adsorbed on a Ag nanoparticle[33–35], while the nanoparticle grows as a result of the reduction of silver ions in solution to their neutral state[36].

Several key studies of chemical processes induced by hot electrons and hot holes[34] and driven by surface plasmons are illustrated in Fig. 3. A particularly simple reaction driven by hot electrons is the room-temperature dissociation of H_2 at Au nanoparticle surfaces (Fig. 3a)[31,32]. In this case, no side reactions are possible: indeed, H_2 only very weakly physisorbs onto the Au nanoparticle surface, and the presence of a porous oxide layer is needed to increase the accommodation coefficient of H_2 on the Au nanoparticle surface. Because of the high mass of Au atoms, an impinging H_2 molecule does not couple efficiently to the Au phonons and will therefore bounce off the surface without loss of kinetic energy. An oxide coating with a high solubility for H_2 allows more efficient kinetic energy dissipation, and the H_2 molecule will therefore spend more time near the metal surface. Excitation of the Au nanoparticle LSPR provides sufficient energy to populate an H_2 antibonding orbital; a wavelength dependence corresponding to the excitation of the LSPR in this system can be clearly observed. Detection of the dissociated molecule was accomplished by flowing both H_2 and D_2 to the plasmonic catalyst: under illumination, the detection of HD molecules indicated that the dissociation reaction resulting from hot

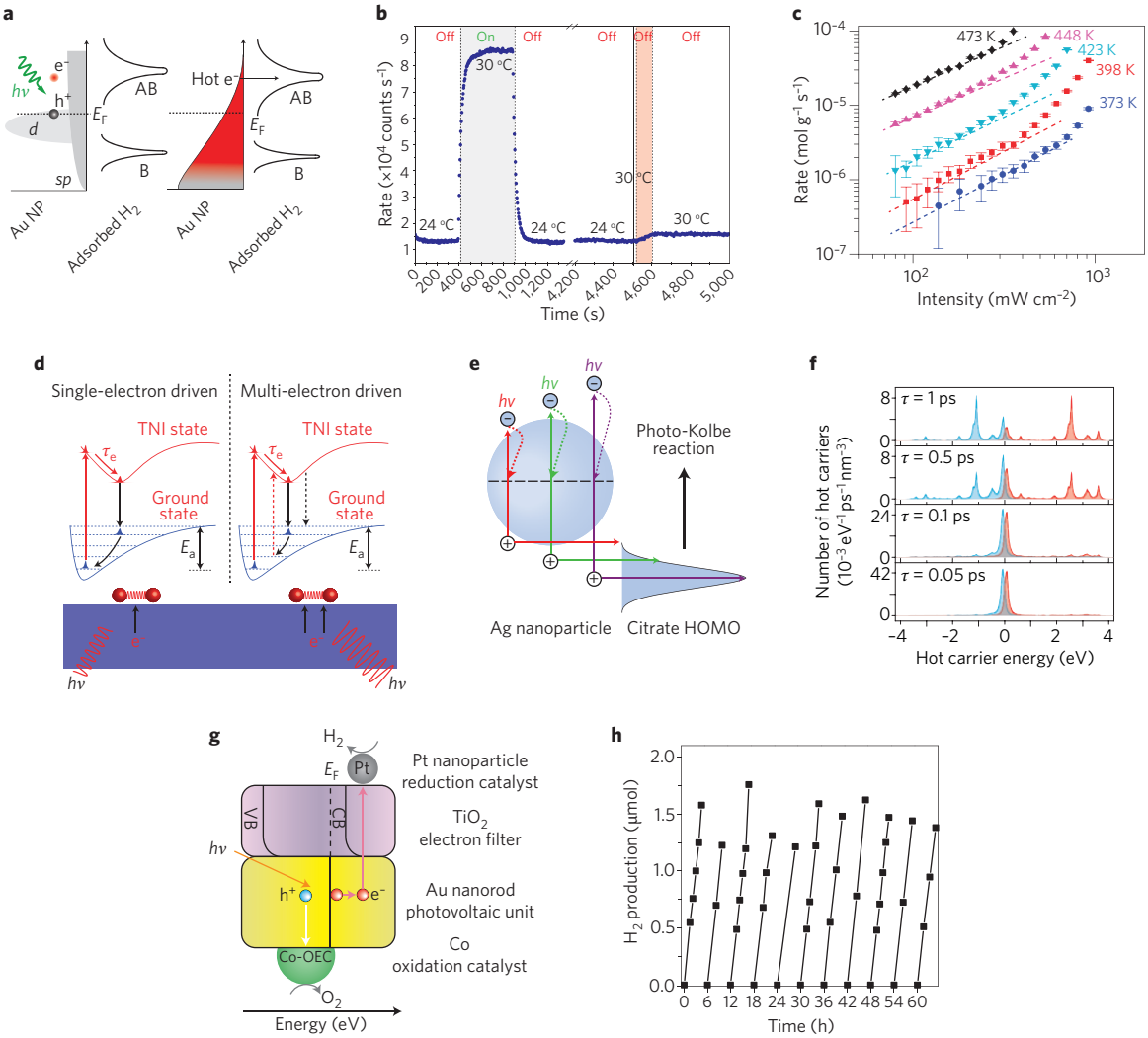

Figure 3 | Examples of hot-carrier-induced chemical processes stimulated by plasmon excitations. a, A schematic depicting the initial step in hot-electron-induced photodissociation of H_2 by transfer of a hot electron into the antibonding orbital of the molecule, resulting in the formation of H_2^- at the Au nanoparticle (NP) surface. AB, antibonding; B, bonding. **b**, A comparison of light-induced HD production (grey) relative to HD produced by the equivalent thermal response with no illumination (red). **c**, The supralinear behaviour of ethylene epoxidation as the incident laser intensity and temperature are both increased. Error bars represent standard deviation. **d**, A schematic depicting O_2 dissociation, the rate-limiting step of the epoxidation reaction in **c**. Supralinear intensity dependence is attributed to multiple attempts by the hot electron to populate the transient negative ion (TNI) state. Single-electron or multi-electron excitations deposit vibrational energy into the adsorbate by accelerating the absorbed molecule for a lifetime, τ_e. If the vibrational energy produced is too low to overcome the activation barrier, E_a, the adsorbate returns to a thermally equilibrated state. **e**, A schematic depicting hot hole transfer from a photoexcited Ag nanoparticle to the highest occupied molecular orbital (HOMO) of a nearby citrate molecule: this transfer results in citrate oxidation, while the negative charge accumulation on the Ag nanoparticle induces reduction of nearby Ag^+ ions, resulting in nanoparticle growth into nanoprisms. **f**, A theoretical calculation of the hot electron (red) and hot hole (blue) distributions in a 15-nm-diameter Ag nanoparticle, with the carrier lifetime (τ) varied between 1 ps and 0.05 ps for an incident light intensity of 1 mW μm^{-2}. **g**, Schematic of an autonomous artificial photosynthesis device where all charge carriers are derived from the hot electrons and holes of surface plasmons. Co-OEC, cobalt oxygen evolution catalyst; CB, conduction band; VB, valence band. **h**, Hydrogen evolution of the water-splitting device shown in **g** driven by solar excitation in 6-h cycles. Figures adapted with permission from: **a**,**b**, ref. 32, © 2012 American Chemical Society; **c**,**d**, ref. 37, 2012 Nature Publishing Group; **e**, ref. 35, © 2013 American Chemical Society; **f**, ref. 5, © 2014 American Chemical Society; **g**,**h**, ref. 38, 2013 Nature Publishing Group.

electron transfer to the transient negative-ion state had occurred. A pronounced difference between light-induced HD formation and a much weaker thermally driven HD population at room temperature provided a clear indication that the process is directly driven by surface plasmons (Fig. 3b). In a follow-on study, the role of the passive oxide layer was examined by substituting the TiO_2 layer with SiO_2, a material with a much higher bandgap. The results confirmed that the oxide layer is only passively involved in the dissociation process; its role is limited to increasing the residence time of H_2 near the metal[31]. In fact, the Au–SiO_2 system features an increase of the reactivity by almost two orders of magnitude over the Au–TiO_2 system, where the conduction band of TiO_2 can serve as an electron acceptor, draining the hot electron supply and thus preventing electron transfer into the antibonding H_2 (or D_2) orbitals.

In a particularly rich set of studies, the hot-electron-driven partial oxidation of ethylene by O_2 to form ethylene oxide was examined[39–41]. This industrially important reaction provides a remarkably simple platform for the study of plasmon-driven photodissociation

of O_2. In this system, the reaction rate is controlled by the dissociation of O_2 to form adsorbed atomic oxygen, followed by a much faster addition of the reactive transient negative-ion species to the double bond of the ethylene molecule[39]. In these studies, the photocatalyst consisted of 60-nm Ag nanocubes, exposing Ag(100) facets for ensuring high reactivity as well as a well-defined plasmon resonance. Several distinguishing properties of plasmonic photocatalysts, relative to conventional semiconductor photocatalysts such as TiO_2, were identified[37]. First, there is a superlinear dependence of the reaction rate on laser intensity (Fig. 3c), indicating that plasmonic photocatalysis can probably be characterized by a positive relationship between quantum efficiency and photon flux, in stark contrast to semiconductor photocatalysts that typically exhibit lower quantum efficiencies as the incident light intensity is increased. Second, the rate and quantum efficiency of photocatalytic reactions on plasmonic nanoparticles increase with temperature, a trend that is opposite to the characteristics of semiconductor photocatalysts. These properties indicate that plasmonic photocatalysts are highly promising for eventual implementation in industrially relevant processes. The studies add new insights to the distribution of energy between the plasmonic catalyst and dissociation of the O_2 adsorbate. More specifically, a kinetic isotope effect (reactivity ratio of $^{16}O_2/^{18}O_2$) of ~1.1 was observed and related to the energy distribution between electronic and vibronic states of the adsorbate due to hot electron transfer from the nanoparticle to the molecule. The kinetic isotope effect increased as a function of the incident light intensity, a behaviour attributed to multiple electronic excitation of the adsorbate molecule before overcoming the activation barrier (E_a) for dissociation (Fig. 3d). These processes work together to increase the overall quantum efficiency of hot-electron-driven O_2 dissociation, that is, the number of product molecules formed per incident photon, as both the operating temperature and incident light intensity are increased. In this specific reaction, at source intensities of 400 mW cm^{-2} and 473 K, the quantum efficiency was nominally 60%, indicating that plasmonic photocatalysts have potential for widespread use in real-world applications. Further improvements and a closer tailoring of plasmonic substrates to specific chemical reactions may result in even higher quantum efficiencies. These examples indicate that plasmonic nanoparticles can be used as substrates for heterogeneous catalysis, as they provide new reaction pathways, the potential for 'soft' (lower energy barriers) chemical reaction conditions, and higher-efficiency reaction rates than those achievable using conventional heterogeneous catalysts.

In addition to plasmon-induced transfer of hot electrons to antibonding adsorbate orbitals, the reverse process is also possible. In a 'hot-hole-driven' process, electrons transfer from occupied adsorbate orbitals to transiently unoccupied states below E_F in the metal. In particular, the surprising discovery that Ag nanoprism synthesis is a process controlled by resonant plasmon excitation is a prime example of hot-hole-driven chemistry[42]. In this reaction, the reduction of the metallic nanoparticle results from the oxidation of citrate ions present in solution[34]. Under resonant illumination, electrons are transferred from the citrate ions to the Ag nanoparticles, which thus acquire a net negative charge. When Ag^+ ions are present in solution, Coulomb forces cause the reduction of the ions at the nanoparticle surface, resulting in nanoparticle growth. Interestingly, the plasmon-induced growth process does not track the nanoparticle plasmon resonance, but rather, increases monotonically with increasing incident photon energy. It is believed that as the photon energy is increased, so is the oxidizing power of the hot hole, offsetting the decrease in the nanoparticle's absorption cross-section (Fig. 3e). The lack of a strong wavelength-dependent response is fortuitous, as nanoparticle growth would result in an inevitable plasmon redshift that, depending on incident photon energy, could self-limit the nanoparticle growth process. Although this study is one of the very few that has elucidated fundamental properties of hot-hole-driven chemistry, it is important to note that this type of reaction could be used broadly in various contexts of oxidation chemistry.

The demonstration of both hot-electron- and hot-hole-driven photochemistry leads to new and more detailed questions about the hot carrier generation process, as well as the properties of plasmon-excited hot carriers. If one was able to design nanoparticle substrates with high yields of hot electrons and/or hot holes at specific energies, it could be possible to optimize a given plasmonic nanoparticle substrate for maximal quantum yield for a specific chemical reaction of interest. The potential fulfilment of this important quest for the chemistry community has stimulated theoretical interest in the investigation of hot carrier properties in metallic nanoparticles. Recent investigations have begun to examine the microscopic origin of the hot carrier generation process[5,43,44]. Results from one such investigation are shown in Fig. 3f, which shows the energy distribution for hot electrons and holes for a 15-nm-diameter Ag nanoparticle. Describing the conduction electrons in a metal as free particles in a spherical potential well, the plasmon-induced hot carrier production was calculated using Fermi's golden rule. As the hot carrier lifetime is not known experimentally, it was used as a parameter in the calculation: carrier lifetimes were varied from τ = 1.0 ps to 0.05 ps, consistent with the range of electron excitation lifetimes reported for extended metallic surfaces[5]. This series of calculations indicates just how sensitively the hot carrier distribution during continuous illumination of the nanoparticle depends on the carrier lifetime. For longer carrier lifetimes, plasmon decay results in 'very hot' electrons (energies high above the Fermi energy of the metal), whereas for shorter carrier lifetimes, the energies of the carriers are closer to the Fermi energy of the metal. Larger-diameter nanoparticles favour generation of less 'hot' carriers. This calculation is also consistent with observations that relate higher hot-electron-based chemical reactivities to smaller nanoparticles, but well-controlled, systematic experimental studies of these effects are clearly needed.

A grand challenge for which plasmon-induced hot carriers may be particularly well suited, and which has recently received considerable interest, is in the harvesting of solar energy for direct generation of alternative fuels. The origin of this work was the initial discovery that n-type TiO_2 electrodes, under ultraviolet illumination, could split water photoelectrochemically[25]. Subsequent efforts to incorporate resonant plasmonic nanoparticles into this process or to reshape the high-index photocatalysts into optically resonant nanostructures has resulted in increased light absorption at the catalyst surface and substantially increased reaction rates[45–47]. More recently, new insights have emerged regarding how to harness plasmon-induced hot carriers for water splitting[48,49]. Of particular significance is the recent work that combines both plasmon-induced hot electron and hole generation in the same integrated device, to produce an artificial photosynthesis device in which all charge carriers derive from surface plasmons[38]. A schematic of this device is shown in Fig. 3g. The uniform array of aligned nanorods that serve as antennas is capped with a crystalline TiO_2 layer resulting in a Schottky barrier. Atop the TiO_2 layer of the nanorod is a layer of Pt nanoparticles, and on the side of each nanorod in the array a cobalt oxygen evolution catalyst is deposited. When light is incident on each nanorod, the hot electrons and the hot holes perform different functions. The hot electrons are injected over the Schottky barrier between the metal and the n-type TiO_2 capping layer, into the conduction band of the TiO_2. Because of the small dimensions of the TiO_2 layer, the hot electrons remain in the conduction band and encounter the Pt nanoparticle layer at the TiO_2 surface. When immersed in water, the Pt nanoparticle layer emits the electrons, functioning as a reduction site for the evolution of H_2. The hot hole, on the other hand, is transported to the cobalt oxygen evolution catalyst, resulting in the local generation of O_2. This clever design shows a greater degree of integration than ever before seen in photoelectrochemical water-splitting devices, with both half-reactions

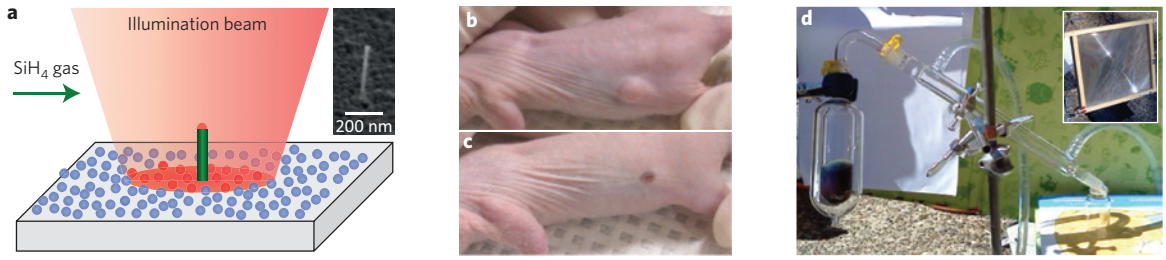

Figure 4 | Physics and applications of hot-electron-induced heating. a, Schematic illustration of a plasmon-assisted nanowire growth procedure in which a low-power, continuous-wave laser is used to heat catalytically active, light-absorbing, metallic nanoparticles (catalyst) to induce the growth of semiconductor nanowires or carbon nanotubes. Inset: Scanning electron microscopy image of an individual silicon nanowire. **b**,**c**, Photographs of a mouse with a subcutaneous prostate cancer tumour on day of treatment by photothermal cancer therapy (**b**), and of the same mouse, 10 days post-treatment, showing full remission of tumour (**c**). **d**, Solar distillation apparatus. The inset shows the Fresnel lens used to focus sunlight. Figures reproduced with permission from: **a**, ref. 68, © 2007 American Chemical Society; **b**,**c**, ref. 79, © 2008 Elsevier; **d**, ref. 80, © 2013 American Chemical Society.

mediated on the same nanorod in different, highly specific regions of the nanostructure. The device runs optimally under AM1.5 illumination, and under constant illumination can evolve hydrogen for more than 66 h without a decrease in activity (Fig. 3h). Although we can expect further optimization, this general device strategy[50] provides a platform for the practical utilization of plasmon-induced hot carriers for the production of alternative sustainable fuels.

We close this subsection by mentioning other types of hot-carrier-induced transformations than chemical reactions. For example, plasmon-induced hot electrons can be injected into a nearby graphene sheet and accomplish significant n-doping[51]. Hot carrier injection can also generate phase transitions in a nearby quantum phase-changing material such as VO_2 (ref. 52) or single-layer MoS_2 (ref. 53). A recent experiment suggests that hot carrier generation may induce a magnetic phase transition in metallic nanocolloids[54]. Such optically controllable phase transformations may open up new avenues for active ultrafast plasmonic devices.

Local heating with hot carriers

The internal decay of hot electrons inside a metallic nanoparticle can lead to significant heating of the nanostructure itself and its immediate environment (Fig. 2c,d)[55–58]. The ability to effectively heat and measure[59–61] the nanostructure's temperature has resulted in many practical plasmonics applications, including selective identification and killing of cancer cells[62], photothermal nanotherapeutics[63], modification of polymer surfaces[64], local control over phase transitions[65,66], growth of individual semiconductor nanowires and carbon nanotubes[67,68], nanofluidics and chemical separation[69], heterogeneous catalysis[70,71], drug delivery[72], photothermal melting of DNA[73–75], and steam generation[76].

We illustrate these exciting opportunities with a few representative examples. Figure 4a shows how light can be used to grow a silicon nanowire from a gold catalyst particle by chemical vapour deposition[77,78]. Typically such wires are grown in a globally heated tube furnace with silane (SiH_4) as the reactant gas and at a temperature above the melting temperature of a Au–Si eutectic alloy (363 °C). Here, the Au catalyst particle was directly heated with a focused laser beam with a wavelength of 532 nm, close to the surface plasmon resonance of the particle. Individual, single-crystal nanowires could be grown (Fig. 4d, inset) using a laser power comparable to that of a laser pointer (a few milliwatts), suggesting a highly energy-efficient pathway to fabricate nanowire devices.

A potentially transformative application of localized heating due to resonant illumination of plasmonic nanoparticles is photothermal cancer therapy. This type of therapy requires the use of nanoparticles whose plasmon resonances are tuned to the near-infrared spectral region, where light absorption by tissue is minimal. Near-infrared resonant nanoparticles are injected into the organism, where they circulate and are taken up into a tumour over the span of several hours[81]. The tumour is then illuminated with resonant light, and the localized photothermal heating induces cellular hyperthermia, resulting in cell death and tumour remission (Fig. 4b,c)[79]. A similar effect can be demonstrated using solutions of broadband absorber nanoparticles, such as nanoshells, and solar irradiation[80]. By focusing sunlight onto a nanoparticle solution, steam can be generated at remarkably high efficiencies (over 80%) with only a minimal heating of the bulk fluid. By dispersing nanoparticles into a fluid mixture, the components can be separated by distillation using sunlight alone (Fig. 4d)[80]. In the case of an ethanol–H_2O mixture, for example, solar distillation yields a distillate richer in ethanol than can be achieved with conventional distillation. The mechanism of this localized heating effect, both in tumours and in fluids, is due to a light-trapping effect induced by incident photons scattering from multiple nanoparticles before an absorption event[81].

In the above-mentioned applications, the need to heat only locally rather than globally has resulted in great increases in control, speed and energy efficiency with an accompanying reduction in cost.

Hot carrier devices

Photovoltaic devices that rely on photoexcitation and the subsequent separation of electron–hole pairs have dominated the photodetector and solar cell markets. The great success of this approach is lessened only by the fact that photons with energies below the semiconductor bandgap cannot be detected or harvested. One can circumvent this challenge by harvesting the energy of photoelectrons ejected from a metal. Just one year after Hertz's discovery of the photoelectric effect, Alexander Stoletov built the first photoelectric cell based on this principle[82]. This led to the development of photodetectors capable of detecting electrons that are photoejected from a metal over either a Schottky[83–87] or oxide tunnel-barrier[88,89].

The band diagram in Fig. 5a illustrates how light absorption in a metal can produce hot electrons that can be emitted over a Schottky barrier (ϕ_B) to produce current. In infrared photodetectors, responsivities as high as 0.25 A W^{-1} (quantum efficiency ≈ 20%) for free-space wavelengths of 1.5 μm have been reported at liquid nitrogen temperatures[90]. Lower barriers afford higher quantum efficiencies but give rise to an increased dark current so that operation at cryogenic temperatures is required.

A challenge in achieving high efficiencies is related to the efficient collection of the excited hot electrons. First attempts to quantify the current from photoejected electrons were made by Fowler[91] and Spicer[92,93]. Spicer intuitively described the internal photoemission process from a metal film as proceeding via a series of three consecutive steps (Fig. 5a). In step 1, hot electrons are generated in the metal through the absorption of a photon. In this process electrons are lifted from states below the Fermi level by the pertinent photon

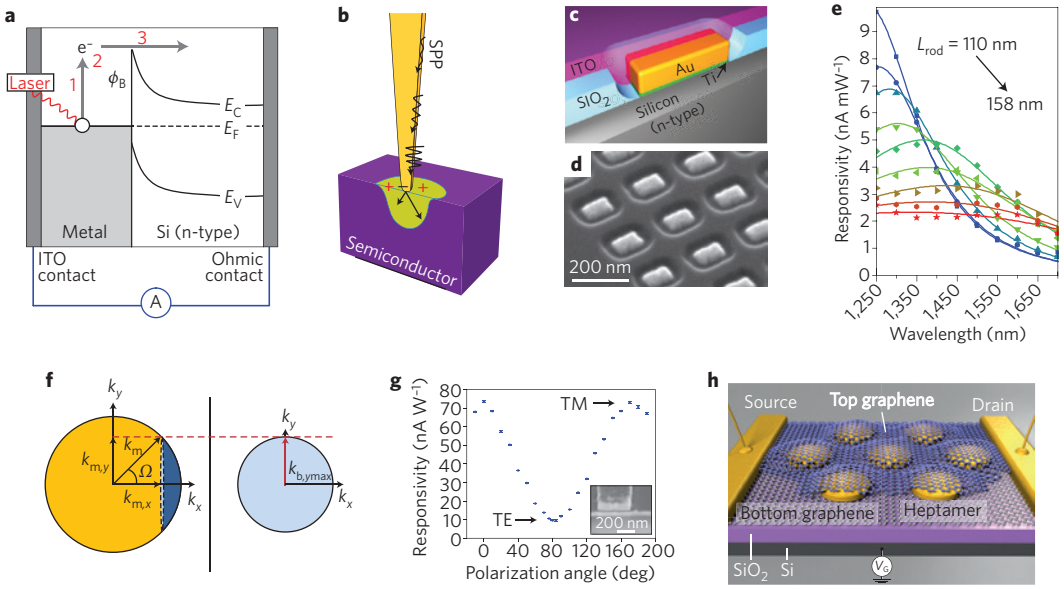

Figure 5 | Hot electron devices. a, Band diagram of a Schottky detector. ITO, indium tin oxide. **b**, Gold taper used to adiabatically compress a surface plasmon polariton (SPP) into the Au/Si Schottky junction. **c**, Gold resonant antenna on an n-type Si substrate. **d**, Scanning electron microscopy image of the device shown in **c** with many Au antennas. **e**, Experimental photocurrent spectra for devices as in panels **c** and **d** with antenna lengths in the range from 110 to 158 nm. **f**, Constant-energy contours for hot electrons in the metal and barrier regions. Hot electron emission is confined to a solid angle Ω that is determined by the maximum allowed momentum of hot electrons in the barrier $k_{b,ymax}$. k_m, hot electron momentum in the metal. **g**, Variation of photoresponsivity with polarization angle for a metal–insulator–metal (MIM) crossbar junction formed between a metal stripe and a planar bottom electrode. TM and TE are the transverse magnetic and electric modes, respectively. The inset shows a scanning electron microscopy image of the device. **h**, Photodetector device consisting of a heptamer plasmonic nanoantenna sandwiched between two graphene layers. Figures reproduced with permission from: **a**,**c**,**d**,**e**, ref. 106, © 2011 American Association for the Advancement of Science; **b**, ref. 104, 2013 Nature Publishing Group; **f**,**g**, ref. 98, © 2014 American Chemical Society; **h**, ref. 109, © 2012 American Chemical Society.

energy $h\nu$. In step 2, some of the hot electrons will move towards the metal/oxide interface. For a first-order estimate of the efficiencies, it is often assumed that the generated hot electrons behave as free electrons and that their initial momentum distribution is isotropic. The latter seems a reasonable initial assumption based on the large mismatch between the wavevectors of the light/surface plasmon and the generated hot electron[94,95]. Although such an analysis may be relevant for semi-infinite planar interfaces, it cannot be straightforwardly extended to nanostructured interfaces or finite nanoparticles[43,96–98]. For such systems, the hot carriers are not free particles but bound to the nanostructure. Momentum conservation does not apply, and a more rigorous treatment accounting for the electron dispersion in the metal should be used to improve the accuracy of hot electron collection efficiency. Nevertheless, only some of the hot carriers will make it to the interface without undergoing inelastic collisions. A physical estimate of this fraction is provided by the mean free path of the electrons, which in metals and semiconductors is quite short (about 1–100 nm) and follows a more-or-less universal dependence on the energy above the Fermi level[99]. The hot electrons arriving at the metal/oxide interface with a kinetic energy exceeding the barrier ϕ_B have a certain probability of traversing the barrier (step 3) but can still be reflected. This follows from the requirement that the electrons have to conserve their energy, and, in the case of a planar interface separating two identical materials, their momentum tangential to the metal/barrier interface upon transmission through the barrier. This can be understood by analysing the constant energy contour that connects all of the possible terminations of the allowed electron momenta at a given kinetic energy

$$E_{kin} = \frac{\hbar^2}{2m_e^*}(k_{i,x}^2 + k_{i,y}^2)$$

where $\hbar$ is reduced Planck's constant, m_e^* is the effective mass of the electron, and $k_{i,x}$ and $k_{i,y}$ are the hot electron momenta in either the metal (i = m) or barrier (i = b) in the x and y directions respectively. For free electron materials, these contours are circles (Fig. 5f). The high Fermi level of common metals and the band offset with the barrier material result in a difference in size of the two circles. This restricts the momenta of the hot electrons that can escape to a solid angle Ω beyond which total internal reflection occurs. Electrons within that solid angle can experience significant reflection as a result of the large wavevector contrast (that is, impedance mismatch) between electrons in the metal contact and barrier[100–102]. It was proposed that roughening the metal/semiconductor surface or using sharp tips can alleviate the issue surrounding the impedance mismatch, and experimentally roughened surfaces have indeed produced higher photocurrents[103,104]. A recent investigation on tapered and nanostructured tips has demonstrated internal quantum efficiencies up to 30%[104]. This hints at the exciting opportunity to engineer optics-inspired, atomic-scale anti-reflection coatings, resonant tunnelling structures and other such structures to manipulate the electrons with characteristic wavelengths of the Fermi wavelength. Another approach to boost efficiency is to increase the interaction length of the metal in metal-clad semiconductor waveguides[103,105] or use optical antennas (Fig. 5d,e)[106–108] capable of concentrating the light absorption near metal/semiconductor interfaces. Optical antennas also allow spectral tuning of the detectors (Fig. 5e).

Similar arguments hold for metal–insulator–metal (MIM) junctions. Thin-film, integrated MIM junctions have been developed as detector elements in the terahertz and mid-infrared ranges since the 1970s[88,89]. At these low frequencies, photoejected carriers cannot make it over the high energetic barriers (~1 eV) typically found in the MIM junctions. For this reason, one typically makes the oxide sufficiently thin (~1 nm) to allow for barrier tunnelling. In the visible or

ultraviolet, an alternative approach based on hot electron generation in one of the metal contacts[110] and its subsequent transport across the oxide to the other metal can be used[111]. Because of the arguments above, the efficiency of hot electron production and emission across the barrier has been too low for practical application[112], and again plasmon excitations have only recently been explored to boost efficiency[102,113]. Recent experiments have also indicated the possibility of directing hot electrons along the polarization of the incident light by exciting surface plasmons[102,107,110]. This can, for example, be seen in the strong polarization dependence of the responsivity of plasmonic MIM detectors where one of the metals was reshaped into a plasmonic stripe-antenna. The large polarization dependence in this case could not be explained by the comparatively small difference in light absorption for the two polarizations along or orthogonal to the stripes (Fig. 5g).

There are also exciting opportunities to realize new functionalities. For example, it was illustrated how the wavelength- and voltage-dependent transmission of hot electrons across a barrier can be exploited to perform spectrometry without the need for spatial dispersion of the light[114]. Recently, very efficient capture of hot electrons emitted by optical antennas was also demonstrated with graphene, further opening the materials suite for hot electron detectors (Fig. 5h)[109]. The fusion of the two-dimensional materials field with the hot carrier field opens up entirely new device functions by capitalizing on the electrically controllable optical and electronic properties of such atomically thin materials.

Outlook

This Review highlights a wealth of opportunities for the generation and use of plasmon-induced hot carriers in nanoparticles. Judiciously designed plasmonic nanostructures can greatly enhance light absorption and convert incident photons into hot electrons and holes with tunable energies[5,43]. This provides tantalizing opportunities for driving out-of-equilibrium physical and chemical processes using hot carriers and offering an extreme degree of control over their energies, temporal features and spatial distribution including, for instance, the specific facet or step-edge from where they are ejected[38,39].

Although the feasibility of plasmon-induced hot carrier generation has been clearly demonstrated in several of the studies highlighted in this Review, further fundamental studies are needed to optimize these processes for viable technological applications. In particular, it will be important to determine with more accuracy the timescales involved in hot carrier relaxation and what physical and chemical parameters influence these timescales.

Timescales play a fundamental role in determining the energy distribution of the hot carriers and thus their probability of transferring into nearby acceptor levels or inducing chemical reactions. It is clear that the increased confinement in a finite nanoparticle will increase the lifetimes of excited carriers compared with the situation on extended surfaces, but the extent of this effect has not been investigated. Because hot electron transfer across Schottky barriers, as discussed in the section 'Hot carrier devices', has been observed experimentally[86,103–106], it follows that a substantial number of hot carriers survive long enough for charge transfer processes to occur. The experiments on plasmon-induced H_2 dissociation, discussed in the section on 'Applications of hot carriers in chemistry', show that hot electrons with energies more than 1 eV above the Fermi level are present[31,32]. Because a dissociation event occurs on a picosecond timescale, the lifetimes of these very hot carriers must exceed this picosecond timescale for dissociation to occur. Although the phase-space argument inherent in Fermi liquid theory suggests that the lifetime of excited electrons depends inversely on the square of their excitation energy (measured from the Fermi level), this argument fails when the excitation energy is large and the dispersion of the electrons is different from electrons on the Fermi surface. Electrons only interact strongly when their wavefunctions overlap. This overlap is typically reduced when the energy difference between the electrons is large. For the same reason, high-energy electrons are unlikely to interact strongly with phonons.

On the topic of plasmon-induced photocatalysis, any fundamental insight gained into the yield and energy distribution of hot carriers will prove invaluable in exploiting these effects for new chemical reactions. It is important to remember that although this field is called 'catalysis' for historical reasons, the role of plasmonic substrates as sources of hot electrons and holes goes far beyond the traditional definition of a catalytic substrate: an entity that influences the rate of reaction but does not change its outcome. As an active contributor of a reactant — electron or hole — in a chemical process, the plasmonic substrate can result in an altogether new set of reaction products, not just a change in reaction rate. The opportunity to use plasmon-induced photochemistry to streamline chemical reactions to favour a specific product is only one tantalizing possibility: facilitating 'impossible' chemical reactions may be a recurrent theme, once the full potential of these hot carrier sources is better understood. Local heating may offer a different lever to control such reactions.

The experimental determination of the timescale for hot carrier relaxation will clearly go beyond conventional 'plasmonic' spectroscopies and will require ultrafast tools and, quite possibly, similar types of ultrahigh-vacuum instrument to those used in surface science. The successful realization of plasmon-induced hot electron science is also highly likely to involve new, non-traditional plasmonic materials that allow more efficient hot carrier production yields than noble metals. In addition to important applications such as photodetection, photocatalysis and light harvesting, plasmon-induced processes are also expected to provide new fundamental insight into dynamical processes at surfaces, including desorption of molecules and chemical reactions. Plasmons are intrinsically ultrafast excitations, and by coupling hot carrier generation on the surfaces of nanoparticles to excitations in nearby systems, such timescales can naturally be probed. Such studies will require new types of time-dependent chemical and physical modelling of quantum mechanical processes and many-electron interactions. To fully capitalize on the many open opportunities, we still have much to learn about hot carriers after more than 125 years of study. With the advances in nanotechnology and nanoscale characterization, this field is ripe for scientific breakthroughs and will remain a hot topic for years to come.

Received 18 July 2014; accepted 24 November 2014;
published online 6 January 2015

References

1. Hertz, H. Ueber einen Einfluss des ultravioletten Lichtes auf die electrische Entladung. *Ann. Phys. Chem.* **267,** 983–1000 (1887).
2. Einstein, A. Über einen die Erzeugung und Verwandlung des Lichtes betreffenden heuristischen Gesichtspunkt. *Ann. Phys.* **322,** 132–148 (1905).
3. Planck, M. Ueber das gesetz der energieverteilung im normalspectrum. *Ann. Phys.* **309,** 553–563 (1901).
4. Hüfner, S. *Photoelectron Spectroscopy: Principles and Applications* (Springer, 2003).
5. Manjavacas, A., Liu, J., Kulkarni, V. & Nordlander, P. Plasmon-induced hot carriers in metallic nanoparticles. *ACS Nano* **8,** 7630–7638 (2014).
This paper proposes a theoretical model that shows how hot carrier production rate and energy distribution depend on the particle size and hot carrier lifetime.
6. Clavero, C. Plasmon-induced hot-electron generation at nanoparticle/metal-oxide interfaces for photovoltaic and photocatalytic devices. *Nature Photon.* **8,** 95–103 (2014).
7. Hofmann, J. & Steinmann, W. Plasma resonance in the photoemission of silver. *Phys. Status Solidi* **30,** K53–K56 (1968).

8. Sipe, J. E. & Becher, J. Surface-plasmon-assisted photoemission. *J. Opt. Soc. Am.* **71,** 1286–1288 (1981).
9. Bohren, C. F. How can a particle absorb more than the light incident on it? *Am. J. Phys.* **51,** 323–327 (1983).
A key paper in plasmonics, which illustrates how subwavelength metallic nanoparticles can absorb light very effectively.
10. Oldenburg, S., Averitt, R., Westcott, S. L. & Halas, N. J. Nanoengineering of optical resonances. *Chem. Phys. Lett.* **288,** 243–247 (1998).
11. Moskovits, M. Surface enhanced spectroscopy. *Rev. Mod. Phys.* **57,** 783–826 (1985).
12. Gersten, J. I. & Nitzan, A. Photophysics and photochemistry near surfaces and small particles. *Surf. Sci.* **158,** 165–189 (1985).
13. Bharadwaj, P., Deutsch, B. & Novotny, L. Optical antennas. *Adv. Opt. Photon.* **1,** 438–483 (2009).
14. Li, X., Xiao, D. & Zhang, Z. Landau damping of quantum plasmons in metal nanostructures. *New J. Phys.* **15,** 023011 (2013).
15. Hao, F. *et al.* Symmetry breaking in plasmonic nanocavities: subradiant LSPR sensing and a tunable Fano resonance. *Nano Lett.* **8,** 3983–3988 (2008).
16. Watanabe, K., Menzel, D., Nilius, N. & Freund, H-J. Photochemistry on metal nanoparticles. *Chem. Rev.* **106,** 4301–4320 (2006).
17. Lisowski, M. *et al.* Ultra-fast dynamics of electron thermalization, cooling and transport effects in Ru(001). *Appl. Phys. A Mater. Sci. Process.* **78,** 165–176 (2004).
18. Inouye, H., Tanaka, K., Tanahashi, I. & Hirao, K. Ultrafast dynamics of nonequilibrium electrons in a gold nanoparticle system. *Phys. Rev. B* **57,** 11334–11340 (1998).
19. Frischkorn, C. & Wolf, M. Femtochemistry at metal surfaces: Nonadiabatic reaction dynamics. *Chem. Rev.* **106,** 4207–4233 (2006).
20. Damascelli, A. *et al.* Fermi surface, surface states, and surface reconstruction in Sr_2RuO_4. *Phys. Rev. Lett.* **4,** 2–5 (2000).
21. Dombi, P. *et al.* Ultrafast strong-field photoemission from plasmonic nanoparticles. *Nano Lett.* **13,** 674–678 (2013).
This paper shows how plasmonic nanoparticles can be used to control photoemission and acceleration of electrons.
22. Buntin, S., Richter, L., Cavanagh, R. & King, D. Optically driven surface reactions: Evidence for the role of hot electrons. *Phys. Rev. Lett.* **61,** 1321–1324 (1988).
23. Bonn, M. *et al.* Phonon- versus electron-mediated desorption and oxidation of CO on Ru(0001). *Science* **285,** 1042–1045 (1999).
24. Kao, F-J., Busch, D. G., Gomes da Costa, D. & Ho, W. Femtosecond versus nanosecond surface photochemistry: O_2+CO on Pt(111) at 80 K. *Phys. Rev. Lett.* **70,** 4098–4101 (1993).
25. Fujishima, A. & Honda, K. Electrochemical photolysis of water at a semiconductor electrode. *Nature* **238,** 37–38 (1972).
26. Kamat, P. V. Photophysical, photochemical and photocatalytic aspects of metal nanoparticles. *J. Phys. Chem. B* **106,** 7729–7744 (2002).
27. Nitzan, A. & Brus, L. E. Theoretical model for enhanced photochemistry on rough surfaces. *J. Chem. Phys.* **75,** 2205–2214 (1981).
28. Brus, L. Noble metal nanocrystals: Plasmon electron transfer photochemistry and single-molecule Raman spectroscopy. *Acc. Chem. Res.* **41,** 1742–1749 (2008).
29. Gavnholt, J., Rubio, A., Olsen, T., Thygesen, K. & Schiøtz, J. Hot-electron-assisted femtochemistry at surfaces: A time-dependent density functional theory approach. *Phys. Rev. B* **79,** 195405 (2009).
30. Ertel, K. *et al.* Time-resolved two-photon photoemission spectroscopy of HOPG and Ag nanoparticles on HOPG. *Appl. Phys. B* **68,** 439–445 (1999).
31. Mukherjee, S. *et al.* Hot-electron-induced dissociation of H_2 on gold nanoparticles supported on SiO_2. *J. Am. Chem. Soc.* **136,** 64–67 (2014).
32. Mukherjee, S., Libisch, F. & Large, N. Hot electrons do the impossible: Plasmon-induced dissociation of H_2 on Au. *Nano Lett.* **13,** 240–247 (2012).
This paper demonstrates that dissociation of H_2 on gold nanoparticles can be accomplished at room temperature, despite a large activation energy.
33. Jin, R., Cao, Y., Hao, E. & Métraux, G. Controlling anisotropic nanoparticle growth through plasmon excitation. *Nature* **425,** 487–490 (2003).
34. Wu, X., Thrall, E. S., Liu, H., Steigerwald, M. & Brus, L. Plasmon induced photovoltage and charge separation in citrate-stabilized gold nanoparticles. *J. Phys. Chem. C* **114,** 12896–12899 (2010).
35. Thrall, E. S., Preska Steinberg, A., Wu, X. & Brus, L. E. The role of photon energy and semiconductor substrate in the plasmon-mediated photooxidation of citrate by silver nanoparticles. *J. Phys. Chem. C* **117,** 26238–26247 (2013).
36. Lee, S. J., Piorek, B. D., Meinhart, C. D. & Moskovits, M. Photoreduction at a distance: facile, nonlocal photoreduction of Ag ions in solution by plasmon-mediated photoemitted electrons. *Nano Lett.* **10,** 1329–1334 (2010).
37. Christopher, P., Xin, H., Marimuthu, A. & Linic, S. Singular characteristics and unique chemical bond activation mechanisms of photocatalytic reactions on plasmonic nanostructures. *Nature Mater.* **11,** 1044–1050 (2012).
38. Mubeen, S. *et al.* An autonomous photosynthetic device in which all charge carriers derive from surface plasmons. *Nature Nanotech.* **8,** 247–252 (2013).
39. Christopher, P., Xin, H. & Linic, S. Visible-light-enhanced catalytic oxidation reactions on plasmonic silver nanostructures. *Nature Chem.* **3,** 467–472 (2011).
A very comprehensive study on the role of plasmonic Ag nanoparticles in enhancing hot-electron-driven catalytic oxidation reactions.
40. Linic, S., Christopher, P. & Ingram, D. B. Plasmonic-metal nanostructures for efficient conversion of solar to chemical energy. *Nature Mater.* **10,** 911–921 (2011).
41. Linic, S., Christopher, P., Xin, H. & Marimuthu, A. Catalytic and photocatalytic transformations on metal nanoparticles with targeted geometric and plasmonic properties. *Acc. Chem. Res.* **46,** 1890–1899 (2013).
42. Jin, R. *et al.* Controlling anisotropic nanoparticle growth through plasmon excitation. *Nature* **425,** 487–490 (2003).
43. Zhang, H. & Govorov, A. O. Optical generation of hot plasmonic carriers in metal nanocrystals: The effects of shape and field enhancement. *J. Phys. Chem. C* **118,** 7606–7614 (2014).
An insightful account on hot carrier generation in metal nanostructures versus bulk metals.
44. Govorov, A. O., Zhang, H. & Gun'ko, Y. K. Theory of photoinjection of hot plasmonic carriers from metal nanostructures into semiconductors and surface molecules. *J. Phys. Chem. C* **117,** 16616–16631 (2013).
45. Thimsen, E., Le Formal, F., Grätzel, M. & Warren, S. C. Influence of plasmonic Au nanoparticles on the photoactivity of Fe_2O_3 electrodes for water splitting. *Nano Lett.* **11,** 35–43 (2011).
46. Thomann, I. *et al.* Plasmon enhanced solar-to-fuel energy conversion. *Nano Lett.* **11,** 3440–3446 (2011).
47. Kim, S. J. *et al.* Light trapping for solar fuel generation with Mie resonances. *Nano Lett.* **14,** 1446–1452 (2014).
48. Mubeen, S., Hernandez-Sosa, G., Moses, D., Lee, J. & Moskovits, M. Plasmonic photosensitization of a wide band gap semiconductor: converting plasmons to charge carriers. *Nano Lett.* **11,** 5548–5552 (2011).
49. Lee, J., Mubeen, S., Ji, X., Stucky, G. D. & Moskovits, M. Plasmonic photoanodes for solar water splitting with visible light. *Nano Lett.* **12,** 5014–5019 (2012).
50. DuChene, J. S. *et al.* Prolonged hot electron dynamics in plasmonic-metal/semiconductor heterostructures with implications for solar photocatalysis. *Angew. Chem. Int. Ed.* **53,** 7887–7891 (2014).
51. Fang, Z. *et al.* Plasmon-induced doping of graphene. *ACS Nano* **6,** 10222–10228 (2012).
52. Appavoo, K. *et al.* Ultrafast phase transition via catastrophic phonon collapse driven by plasmonic hot-electron injection. *Nano Lett.* **14,** 1127–1133 (2014).
53. Kang, Y. *et al.* Plasmonic hot electron induced structural phase transition in a MoS_2 monolayer. *Adv. Mater.* **26,** 6467–6471 (2014).
This paper analyses the role of hot electrons in inducing structural phase transformations.
54. Moocarme, M., Domínguez-Juaŕez, J. L. & Vuong, L. T. Ultralow-intensity magneto-optical and mechanical effects in metal nanocolloids. *Nano Lett.* **14,** 1178–1183 (2014).
55. Baffou, G., Quidant, R. & Girard, C. Heat generation in plasmonic nanostructures: Influence of morphology. *Appl. Phys. Lett.* **94,** 153109 (2009).
56. Baffou, G. & Quidant, R. Thermo-plasmonics: using metallic nanostructures as nano-sources of heat. *Laser Photon. Rev.* **7,** 171–187 (2013).
57. Richardson, H. H., Carlson, M. T., Tandler, P. J., Hernandez, P. & Govorov, A. O. Experimental and theoretical studies of light-to-heat conversion and collective heating effects in metal nanoparticle solutions. *Nano Lett.* **9,** 1139–1146 (2009).
58. Baffou, G., Quidant, R. & García de Abajo, F. J. Nanoscale control of optical heating in complex plasmonic systems. *ACS Nano* **4,** 709–716 (2010).
59. Baffou, G., Kreuzer, M. P., Kulzer, F. & Quidant, R. Temperature mapping near plasmonic nanostructures using fluorescence polarization anisotropy. *Opt. Express* **17,** 3291–3298 (2009).
60. Boyer, D., Tamarat, P., Maali, A., Lounis, B. & Orrit, M. Photothermal imaging of nanometer-sized metal particles among scatterers. *Science* **297,** 1160–1163 (2002).
61. Baffou, G. *et al.* Thermal imaging of nanostructures by quantitative optical phase analysis. *ACS Nano* **6,** 2452–2458 (2012).
This paper shows how to control and map temperature with high spatial resolution near metallic nanostructures.
62. Hirsch, L. R. *et al.* Nanoshell-mediated near-infrared thermal therapy of tumors under magnetic resonance guidance. *Proc. Natl Acad. Sci. USA* **100,** 13549–13554 (2003).
A key paper that shows the potential use of plasmonic nanoparticle heating for thermal therapies.
63. Zharov, V. P., Mercer, K. E., Galitovskaya, E. N. & Smeltzer, M. S. Photothermal nanotherapeutics and nanodiagnostics for selective killing of bacteria targeted with gold nanoparticles. *Biophys. J.* **90,** 619–627 (2006).

64. Röntzsch, L., Heinig, K-H., Schuller, J. A. & Brongersma, M. L. Thin film patterning by surface-plasmon-induced thermocapillarity. *Appl. Phys. Lett.* **90,** 044105 (2007).
65. Richardson, H. H., Thomas, A. C., Carlson, M. T., Kordesch, M. E. & Govorov, A. O. Thermo-optical responses of nanoparticles: Melting of ice and nanocalorimetry approach. *J. Electron. Mater.* **36,** 1587–1593 (2007).
66. Soares, B., Jonsson, F. & Zheludev, N. All-optical phase-change memory in a single gallium nanoparticle. *Phys. Rev. Lett.* **98,** 153905 (2007).
67. Boyd, D. A., Greengard, L., Brongersma, M., El-Naggar, M. Y. & Goodwin, D. G. Plasmon-assisted chemical vapor deposition. *Nano Lett.* **6,** 2592–2597 (2006).
This paper demonstrates the use of plasmonic heating to grow nanostructures by chemical vapour deposition.
68. Cao, L., Barsic, D. N., Guichard, A. R. & Brongersma, M. L. Plasmon-assisted local temperature control to pattern individual semiconductor nanowires and carbon nanotubes. *Nano Lett.* **7,** 3523–3527 (2007).
69. Boyd, D. A., Adleman, J. R., Goodwin, D. G. & Psaltis, D. Chemical separations by bubble-assisted interphase mass-transfer. *Anal. Chem.* **80,** 2452–2456 (2008).
70. Adleman, J., Boyd, D., Goodwin, D. & Psaltis, D. Heterogenous catalysis mediated by plasmon heating. *Nano Lett.* **9,** 4417–4423 (2009).
71. Greengard, L., Brongersma, M. & Boyd, D. Electromagnetic control of chemical catalysis. US Patent 7,998,538 (2004).
72. Sershen, S. R., Westcott, S. L., Halas, N. J. & West, J. L. Young Investigator Award World Biomaterials Congress: Temperature-sensitive polymer–nanoshell composites for photothermally modulated drug delivery. *J. Biomed. Mater. Res.* **51,** 293–298 (2000).
73. Stehr, J. *et al.* Gold nanostoves for microsecond DNA melting analysis. *Nano Lett.* **8,** 619–623 (2008).
74. Reismann, M., Bretschneider, J. C., von Plessen, G. & Simon, U. Reversible photothermal melting of DNA in DNA–gold-nanoparticle networks. *Small* **4,** 607–610 (2008).
75. Osinkina, L. *et al.* Tuning DNA binding kinetics in an optical trap by plasmonic nanoparticle heating. *Nano Lett.* **13,** 3140–3144 (2013).
76. Neumann, O. *et al.* Compact solar autoclave based on steam generation using broadband light-harvesting nanoparticles. *Proc. Natl Acad. Sci. USA* **110,** 11677–11681 (2013).
77. Wagner, R. S. & Ellis, W. C. Vapor–liquid–solid mechanism of single crystal growth. *Appl. Phys. Lett.* **4,** 89–90 (1964).
78. Cui, Y., Lauhon, L. J., Gudiksen, M. S., Wang, J. & Lieber, C. M. Diameter-controlled synthesis of single-crystal silicon nanowires. *Appl. Phys. Lett.* **78,** 2214–2216 (2001).
79. Stern, J. M., Stanfield, J., Kabbani, W., Hsieh, J-T. & Cadeddu, J. A. Selective prostate cancer thermal ablation with laser activated gold nanoshells. *J. Urol.* **179,** 748–753 (2008).
80. Neumann, O. *et al.* Solar vapor generation enabled by nanoparticles. *ACS Nano* **7,** 42–49 (2013).
81. Hogan, N., Urban, A. & Orozco, C. A. Nanoparticles heat through light localization. *Nano Lett.* **14,** 4640–4645 (2014).
82. Stoletow, M. On a kind of electrical current produced by ultra-violet rays. *Phil. Mag. Ser. 5* **26,** 317–319 (1888).
83. Peters, D. An infrared detector utilizing internal photoemission. *Proc. IEEE* **55,** 704–705 (1967).
An early work showing the use of hot carrier emission to make photodetectors for low energy, infrared photons.
84. Akbari, A. & Berini, P. Schottky contact surface-plasmon detector integrated with an asymmetric metal stripe waveguide. *Appl. Phys. Lett.* **95,** 021104 (2009).
85. Scales, C. & Berini, P. Thin-film Schottky barrier photodetector models. *IEEE J. Quantum Electron.* **46,** 633–643 (2010).
86. Goykhman, I., Desiatov, B., Khurgin, J., Shappir, J. & Levy, U. Locally oxidized silicon surface-plasmon Schottky detector for telecom regime. *Nano Lett.* **11,** 2219–2224 (2011).
87. Liu, M. & Chou, S. Internal emission metal–semiconductor–metal photodetectors on Si and GaAs for 1.3 μm detection. *Appl. Phys. Lett.* **66,** 2673–2675 (1995).
88. Faris, S., Gustafson, T. & Wiesner, J. Detection of optical and infrared radiation with DC-biased electron-tunneling metal–barrier–metal diodes. *IEEE J. Quantum Electron.* **9,** 737–745 (1973).
89. Heiblum, M., Wang, S., Whinnery, J. R. & Gustafson, T. K. Characteristics of integrated MOM junctions at dc and at optical frequencies. *IEEE J. Quantum Electron.* **14,** 159–169 (1978).
90. Ye, J. *et al.* Accessing the transport properties of graphene and its multilayers at high carrier density. *Proc. Natl Acad. Sci. USA* **108,** 13002–13006 (2011).
91. Fowler, R. The analysis of photoelectric sensitivity curves for clean metals at various temperatures. *Phys. Rev.* **107,** 45–56 (1931).
92. Spicer, W. E. Photoemissive, photoconductive, and optical absorption studies of alkali–antimony compounds. *Phys. Rev.* **112,** 114–122 (1958).
93. Spicer, W. E. Negative affinity 3–5 photocathodes: Their physics and technology. *Appl. Phys.* **12,** 115–130 (1977).
94. Kane, E. Simple model for collision effects in photoemission. *Phys. Rev.* **147,** 335–339 (1966).
95. Dalal, V. L. Simple model for internal photoemission. *J. Appl. Phys.* **42,** 2274–2279 (1971).
96. Govorov, A. O., Zhang, H., Demir, H. V. & Gun'ko, Y. K. Photogeneration of hot plasmonic electrons with metal nanocrystals: Quantum description and potential applications. *Nano Today* **9,** 85–101 (2014).
97. Sobhani, A *et al.* Narrowband photodetection in the near-infrared with a plasmon-induced hot electron device. *Nature Commun.* **4,** 1643 (2013).
98. Chalabi, H., Schoen, D. & Brongersma, M. L. Hot-electron photodetection with a plasmonic nanostripe antenna. *Nano Lett.* **14,** 1374–1380 (2014).
99. Seah, M. P. & Dench, W. A. Quantitative electron spectroscopy of surfaces. *Surf. Interface Anal.* **1,** 2–11 (1979).
100. Gaylord, T. K. & Brennan, K. F. Electron wave optics in semiconductors. *J. Appl. Phys.* **65,** 814–820 (1989).
101. Ilya, G., Boris, D., Shappir, J., Khurgin, J. B. & Levy, U. Model for quantum efficiency of guided mode plasmonic enhanced silicon Schottky detectors. Preprint at http://arXiv.org/1401.2624 (2014).
102. Chalabi, H., Schoen, D. & Brongersma, M. Hot-electron photodetection with a plasmonic nanostripe antenna. *Nano Lett.* **14,** 1374–1380 (2014).
103. Goykhman, I., Desiatov, B., Khurgin, J., Shappir, J. & Levy, U. Waveguide based compact silicon Schottky photodetector with enhanced responsivity in the telecom spectral band. *Opt. Express* **20,** 28594–28602 (2012).
This paper shows the possibility to realize high responsivity photodetectors that are integrated with a Si waveguide.
104. Giugni, A. *et al.* Hot-electron nanoscopy using adiabatic compression of surface plasmons. *Nature Nanotech.* **8,** 845–852 (2013).
105. Scales, C., Breukelaar, I., Charbonneau, R. & Berini, P. Infrared performance of symmetric surface-plasmon waveguide Schottky detectors in Si. *J. Light. Technol.* **29,** 1852–1860 (2011).
106. Knight, M. W., Sobhani, H., Nordlander, P. & Halas, N. J. Photodetection with active optical antennas. *Science* **332,** 702–704 (2011).
This paper demonstrates the use of plasmonic antennas to tune the spectral response of a hot carrier detector.
107. Knight, M., Wang, Y. & Urban, A. Embedding plasmonic nanostructure diodes enhances hot electron emission. *Nano Lett.* **13,** 1687–1692 (2013).
108. Lee, Y., Jung, C., Park, J. & Seo, H. Surface plasmon-driven hot electron flow probed with metal–semiconductor nanodiodes. *Nano Lett.* **11,** 4251–4255 (2011).
109. Fang, Z. *et al.* Graphene-antenna sandwich photodetector. *Nano Lett.* **12,** 3808–3813 (2012).
110. Shalaev, V., Douketis, C., Stuckless, J. & Moskovits, M. Light-induced kinetic effects in solids. *Phys. Rev. B* **53,** 11388–11402 (1996).
111. Kovacs, D., Winter, J., Meyer, S., Wucher, A. & Diesing, D. Photo and particle induced transport of excited carriers in thin film tunnel junctions. *Phys. Rev. B* **76,** 235408 (2007).
112. Burshtein, Z. & Levinson, J. Photo-induced tunnel currents in Al–Al_2O_3–Au structures. *Phys. Rev. B* **12,** 3452–3457 (1975).
113. Atar, F., Battal, E., Aygun, L. & Daglar, B. Plasmonically enhanced hot electron based photovoltaic device. *Opt. Express* **21,** 7196–7201 (2013).
114. Wang, F. & Melosh, N. A. Power-independent wavelength determination by hot carrier collection in metal–insulator–metal devices. *Nature Commun.* **4,** 1711 (2013).

Acknowledgements

We thank all of the students and postdocs in our groups who are actively involved with hot electron research. We also greatly acknowledge support from the DOE Light–Material Interactions Energy Frontier Research Centre, an Energy Frontier Research Centre funded by the US Department of Energy, Office of Science, Basic Energy Sciences under Award DE-SC0001293. P.N. and N.J.H. acknowledge support from the Robert A. Welch Foundation through grants C-1220 and C-1222, and also acknowledge support through the AFOSR MURI programme.

Additional information

Reprints and permissions information is available online at www.nature.com/reprints. Correspondence should be addressed to M.L.B., N.J.H. or P.N.

Competing financial interests

The authors declare no competing financial interests.